Strong Relativistic Effects in Lanthanide-Based Single-Molecule Magnets

Vsevolod D. Dergachev, Daria D. Nakritskaia, and Sergey A. Varganov*

Department of Chemistry, University of Nevada, Reno, 1664 N. Virginia Street, Reno, Nevada 89557-0216, United States

*e-mail: svarganov@unr.edu

ABSTRACT

Lanthanide-based single-molecule magnets (SMMs) are promising building blocks for quantum memory and spintronic devices. Designing lanthanide-based SMMs with long spin relaxation time requires a detailed understanding of their electronic structure, including the crucial role of the spin-orbit coupling (SOC). While traditional calculations of SOC using the perturbation theory applied to a solution of the non-relativistic Schrödinger equation are valid for light atoms, this approach is questionable for systems containing heavy elements such as lanthanides. We investigate the accuracy of the perturbation estimates of SOC by variationally solving the Dirac equation for the $[DyO]^+$ molecule, a prototype of a lanthanide-based SMM. We show that the energy splittings between the M_J states involved in spin relaxation depend on the interplay between strong SOC and dynamic electron correlations. We demonstrate that this interplay affects the resonances between the spin and vibrational transitions, and, therefore, the spin relaxation time.

TOC GRAPHICS

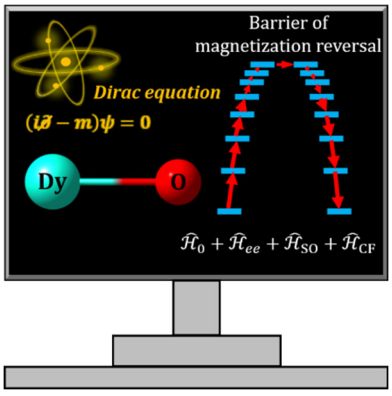

KEYWORDS

magnetic anisotropy, crystal field splitting, spin-orbit coupling, spin-vibrational coupling, perturbation theory, Dirac equation

The design of new lanthanide-based single-molecule magnets (Ln-based SMMs)[1–11] is a very active field of research driven by their potential applications in spintronics[1,12,13] and high-density information storage.[14,15] Magnetic properties of Ln-based SMMs arise from the large electron spin (S) and orbital angular momentum (L) of lanthanide ions. The strong spin-orbit coupling (SOC)[16–22] combines S and L into the total angular momentum (pseudospin) J that defines magnetization of SMMs. To be useful for practical applications, an SMM must be characterized by slow relaxation of magnetization (long pseudospin relaxation time), which requires a strong anisotropy of the crystal field around Ln ion and a minimal coupling between the pseudospin and molecular vibrations.[2,4] Therefore, the design strategy of Ln-based SMMs involves developing ligands that would produce a strong anisotropic environment and reduce couplings between the spin and vibrational states of the resulting complex. This strategy requires an ability to accurately predict energies and spin properties of the low-lying electronic states of potential SMMs using high-level *ab initio* electronic structure calculations. In such calculations, SOC is usually estimated using the perturbation theory applied to a non-relativistic solution of the Schrödinger equation corrected for only the scalar relativistic effects. However, it is not clear if this perturbation approach to SOC is suitable for molecules containing heavy elements, such as lanthanides and actinides.[23] In this work, we address this question by variationally solving the relativistic four- and two-component versions of the Dirac equation for a prototype of Ln-based SMM.

Electronic structure and magnetic properties of Ln-based SMMs can be understood by considering various interactions acting on the *f*-electrons of Ln ion. To be more specific, we consider a Dy^{3+}-based SMM (Figure 1). The one-electron atomic Hamiltonian $\widehat{\mathcal{H}}_0$ predicts the f^9 electron configuration for the Dy^{3+} ion. The addition of the electron-electron interaction $\widehat{\mathcal{H}}_{ee}$ splits this electron configuration into the atomic terms ^{6}H, ^{6}F, ^{6}P, etc., where the letters indicate the values of the orbital angular momentum L and the superscript is the spin multiplicity 2S+1=6 (five unpaired electrons). The SOC $\widehat{\mathcal{H}}_{\mathrm{SO}}$ splits each term into levels with different values of the pseudospin J. For simplicity, only the lowest-energy manifold $^6\mathrm{H_J}$ with J=|L – S|,…,L+S is shown in Figure 1. Finally, each level is split by the interaction with the ligands represented by the crystal field term $\widehat{\mathcal{H}}_{\mathrm{CF}}$. Again, for simplicity, only the 2J+1=16 states originated from the ground level $^6\mathrm{H}_{15/2}$ are shown. For the Kramer ions, which have the odd number of electrons as Dy^{3+}, the crystal field splits each level into a pair of degenerate states characterized by the magnetic quantum number $\pm\mathrm{M_J}$. The magnetic quantum number represents the projection of the pseudospin J on the quantization z-axis. Therefore, the crystal field produces a magnetic anisotropy barrier (U_{A}) for reversal of magnetization. Large U_{A} is required to minimize the over-the-barrier magnetization relaxation corresponding to the pseudospin flipping between the $\mathrm{M_J} = 15/2$ and $\mathrm{M_J} = -15/2$ states. In addition to the over-the-barrier relaxation, the quantum tunneling and the spin-vibrational coupling mediated transitions between different $\mathrm{M_J}$ states also contribute to the overall spin relaxation in Ln-based SMMs.[4–6,8,24–27]

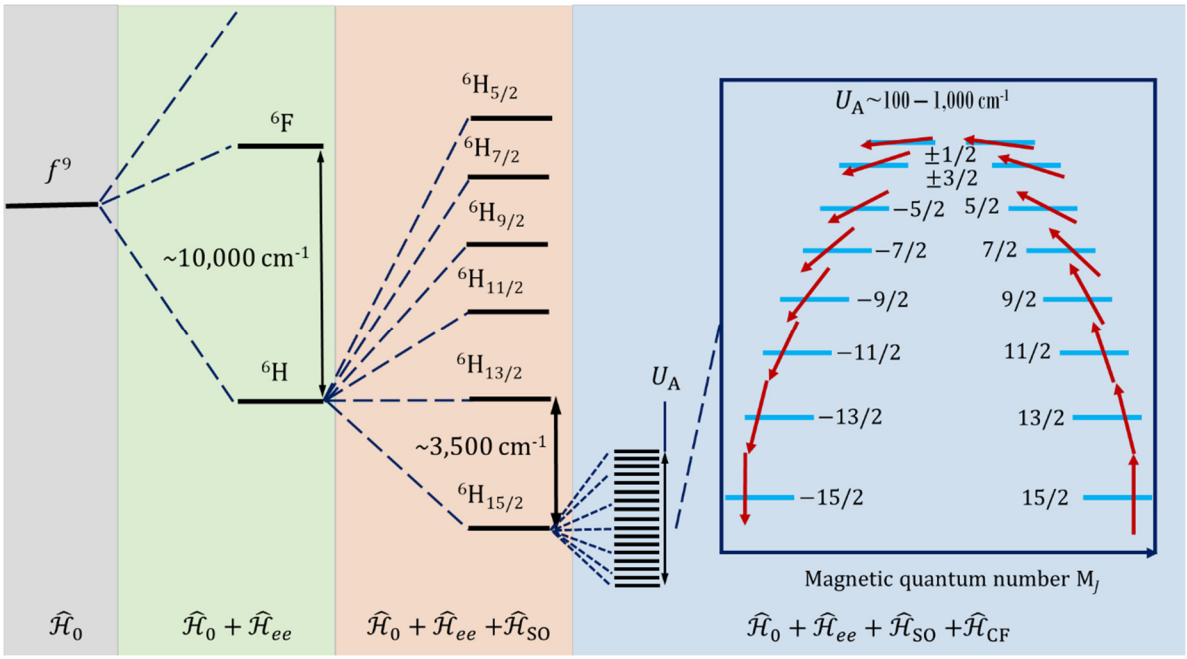

Figure 1. Electronic structure of a Dy^{3+}-based SMM. The magnitude of interactions responsible for splitting of the energy levels increases from left to right ($\hat{\mathcal{H}}_0$ – one-electron atomic Hamiltonian, $\hat{\mathcal{H}}_{ee}$ – electron-electron interaction, $\hat{\mathcal{H}}_{SO}$ – spin-orbit interaction, $\hat{\mathcal{H}}_{CF}$ – crystal field interaction). U_A is the magnetic anisotropy barrier. The red arrows schematically show direction of the pseudospin J for each M_J state.

Calculating SOC accurately is critical for predicting the electronic structure and magnetic properties of Ln-based SMMs. While the traditional approach to estimating SOC with the perturbation theory applied to a non-relativistic solution of the Schrödinger equation works well for molecules containing only light atoms, for heavy elements like lanthanides,[28–30] the use of the perturbative approach is questionable. In this work, we variationally solve the relativistic Dirac equation for the $[DyO]^+$ molecule, a prototype of a Ln-based SMM.[4] The magnetic anisotropy of oblate Ln ions is maximized in an axial crystal field.[2,4] The linear $[DyO]^+$ molecule is an example of an oblate Kramer ion in the perfectly axial field characterized by the doubly degenerate $\pm M_J$ states. We focus on the effects of strong SOC and dynamic electron correlation on the energy splitting between the M_J states and the spin relaxation rate. We compare our results with those obtained using the widely used perturbation approach to calculating SOC.

The variational relativistic electronic structure calculations were performed by solving the Dirac equation in the DIRAC19 package.[31] In this work, we compared the results of the four-component and exact two-component (X2C)[32–37] calculations. Recently, the X2C method has been shown to accurately model the X-ray absorption spectra and intersystem crossing transitions in molecules containing late-row elements.[38,39] In our study, we find that the energy gaps between the M_J states calculated using the four- and two-component methods agree within 9 cm^{-1} (Table S3), indicating the high accuracy of the variational X2C method. We also compare the results of the variational SOC calculations with those obtained using the conventional perturbative SOC approach, as implemented in the GAMESS[40] and OpenMolcas[41] suite of programs. To describe

the static electron correlation arising from the partially occupied quasi-degenerate 4*f* orbitals of Dy^{3+}, we utilized the complete active space self-consistent field (CASSCF) method. The dynamic electron correlations were accounted for with the multireference configuration interaction method with single and double excitations (MRCISD)[42,43], multiconfiguration quasi-degenerate second-order perturbation theory (MCQDPT2),[44] and complete active space second order perturbation theory (CASPT2).[45]

The energies of the M_J states of $[DyO]^+$, which arise from the splitting of $^6H_{15/2}$ level of Dy^{3+}, were calculated using the variational and perturbation approaches and are shown in Figure 2. The energy splittings between the lowest pairs of the M_J states ($M_J = \pm 15/2$ and $\pm 13/2$; $M_J = \pm 13/2$ and $\pm 11/2$) predicted with the variational SOC approach are about 40% larger than those obtained using the perturbation theory. At the room temperature, these larger energy splittings would result in an order of magnitude decrease in the population of the $M_J = \pm 13/2$ states relative to the $M_J = \pm 15/2$ states, and a half order of magnitude decrease in the population of the $M_J = \pm 11/2$ states relative to the $M_J = \pm 13/2$ states. Such large reduction of the excited state populations predicted by the variational approach is expected to suppress the spin relaxation mechanisms that proceed through these states.[25,27] This will lead to the increase of the predicted blocking temperature (T_B),[5] the temperature below which the relaxation of magnetization is slower than the time scale of measurements.

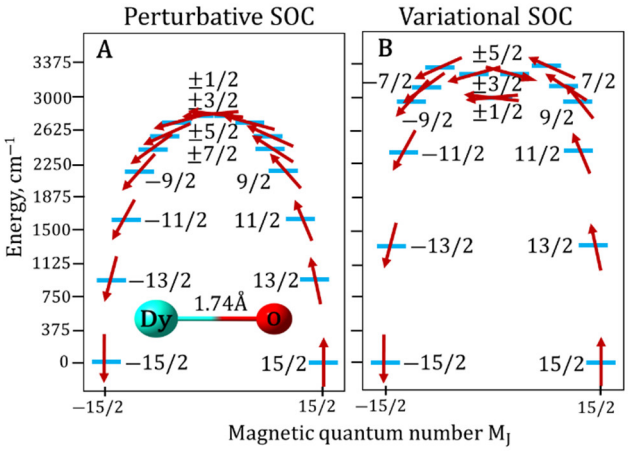

Figure 2. Energies of the M_J states of the $[DyO]^+$ arising from the ground spin-orbit level $^6H_{15/2}$ of Dy^{3+}. The CASSCF state energies are shown for the perturbative SOC (panel A) and X2C (panel B) approaches. The red arrows schematically show the direction of pseudospin J for each M_J state.

In the variational SOC approach, the inclusion of dynamic electron correlation leads to a significant decrease in the energy splittings between the lowest M_J states (Figure S5). In contrast, accounting for dynamic correlation in the perturbative SOC approach results in an increase in the energy splittings. Interestingly, when dynamic electron correlation is accounted for, the energies of M_J states predicted by the variational and perturbative approaches are similar, with an important exception of the first excited $M_J = \pm 13/2$ state whose energy is overestimated in the perturbative approach by 173 cm^{-1} (Figure S6). This indicates a fortunate cancelation of the error arising from treating SOC with perturbation theory and the error produced by accounting for only limited

amount of dynamic electron correlation. This cancelation of errors could be related to the fact that both the SOC and dynamic electron correlation are treated within the framework of the same multiconfigurational quasi-degenerate perturbation theory (MCQDPT2).

We found that the order of the highest electronic states is sensitive to the level of theory (Figure 2, S5 and S6). If only the static electron correlation is included as in the CASSCF method, the variational SOC calculation predicts a deviation from the well-known bell-shape order, in contrast to the perturbative SOC prediction. In addition, for small double-zeta basis the bell-shape order is broken even in the CASSCF results (Table S8). Interestingly, if the dynamic electron correlation is included, the order of the states deviates from the bell shape regardless of the perturbative or variational approach to SOC. This can be explained by analyzing the electron excitations from the highest occupied to the lowest unoccupied molecular orbitals. The lowest unoccupied orbitals in $[DyO]^+$ are characterized by large contributions from the atomic orbitals with small angular momentum (Figure S2), and therefore, the electron excitations to these orbitals stabilize the states with smaller value of M_J, such as $M_J = \pm 1/2$ and $M_J = \pm 3/2$.

At higher temperatures, the magnetization relaxation in SMMs is often dominated by the energy transfer between the spin and vibrational degrees of freedom. Therefore, the spin relaxation rate of a state a can be rationalized using Fermi's golden rule,[46-50]

$$k_a = \frac{2\pi}{\hbar} \sum_b \sum_\alpha \left| \langle b | \hat{V}_\alpha | a \rangle \right|^2 \delta(\omega_{ba} \pm \omega_\alpha), \quad (1)$$

where $\hat{V}_\alpha$ is the spin-vibrational (spin-phonon) coupling[8] along the vibrational normal mode α, ω_{ba} is the frequency that corresponds to the energy gap between the states b and a, and ω_α is the frequency of the normal mode α. The delta function $\delta(\omega_{ba} \pm \omega_\alpha)$ approximates the vibrational density of states at energies $\omega_{ba} \pm \omega_\alpha$, where the minus sign corresponds to the phonon absorption, and the plus sign corresponds to the phonon emission. For a diatomic molecule, such as $[DyO]^+$, Eq. (1) reduces to

$$k_a = \frac{2\pi}{\hbar} \sum_b |\langle b | \mathrm{d}/\mathrm{dR} | a \rangle|^2 \delta(\omega_{ba} \pm \omega), \quad (2)$$

where $\langle b | \mathrm{d}/\mathrm{dR} | a \rangle$ is the spin-vibrational coupling, d/dR is the derivative (nonadiabatic) coupling operator, R is the internuclear distance, and ω is the vibrational frequency. In general, each electronic state is represented as a linear combination of M_J states of an ion. In the axially symmetric systems, such as $[DyO]^+$, the total angular momentum J is conserved and each state is characterized by a specific M_J value, which leads to the vanishing spin-vibrational coupling (see Supporting Information). However, it is still insightful to assess how the variational treatment of SOC affects the resonances between the spin and vibrational transitions, which described by the delta function in Eq. (2). The fundamental vibrational frequency required to estimate the spin-vibrational resonances was obtained by fitting the calculated energies in the vicinity of the equilibrium geometry with the harmonic potential. The anharmonic correction of 7 cm^{-1} was calculated from fitting the energies to the Morse potential. The obtained spectroscopic constants are given in Supporting Information.

The X2C-CASSCF calculations with variational SOC predict that the $M_J = \pm 13/2$ to $M_J = \pm 11/2$ ($\pm 13/2 \leftrightarrow \pm 11/2$) transition is the closest (within 47 cm^{-1}) to the vibrational transition at 988 cm^{-1} (Figure 3A). The transition from the ground state to the first excited state ($\pm 15/2 \leftrightarrow \pm 13/2$) is off resonance with the vibrational transition, indicating that the ground state will not contribute to the spin-vibrational relaxation. Accounting for the dynamic electron correlation with X2C-MRCISD shifts the vibrational transition from 988 to 1086 cm^{-1} and shifts two spin transitions ($\pm 11/2 \leftrightarrow \pm 1/2$ and $\pm 15/2 \leftrightarrow \pm 13/2$) toward the resonance (Figure 3B). Interestingly, the simultaneous shift of the vibrational and ($\pm 13/2 \leftrightarrow \pm 11/2$) spin transitions preserves their proximity to each other (42 cm^{-1} energy difference). The shift of spin transitions toward vibrational frequency indicates that the spin-vibrational resonance conditions are sensitive to dynamic electron correlation. Therefore, to understand the spin relaxation mediated by spin-vibrational coupling, it is important to account for dynamic correlation in the variational SOC calculations.

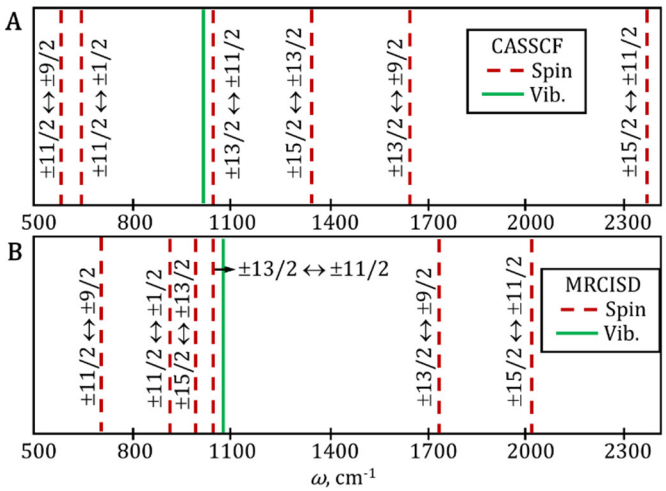

Figure 3. Energies of the vibrational transition (solid green line) and the spin transitions between the M_J states (dashed red lines) in $[DyO]^+$ calculated using the variational SOC approach. The CASSCF transition energies without dynamic electron correlation (panel A) and the MRCISD transition energies with dynamic electron correlation (panel B).

Figure 4 highlights the importance of variational treatment of strong SOC in Ln-based SMMs by comparing the transition energies predicted by the variational (X2C-MRCISD) and traditional perturbative (MCQDPT2) SOC approaches. The first thing to notice is that the perturbative approach underestimates the harmonic vibrational frequency by 243 cm^{-1} compared to the more accurate variational SOC calculation. The perturbative SOC approach strongly affects the spin transition frequencies. Interestingly, this leads to the same near resonance condition between the ($\pm 13/2 \leftrightarrow \pm 11/2$) spin and vibrational transitions as was observed in the variational SOC calculations. Therefore, both vibrational and spin transition frequencies are strongly affected by the variational treatment of SOC. This suggests that for predicting the spin relaxation rate in Ln-based SMMs, the variational treatment of the strong SOC effects is highly desirable.

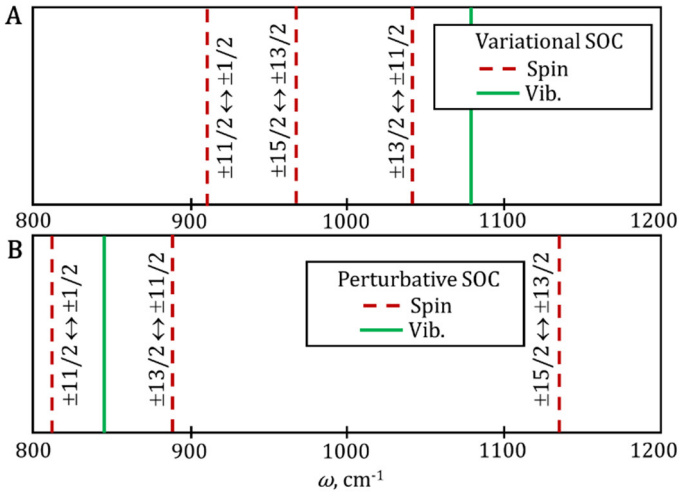

Figure 4. Energies of the vibrational transition (solid green line) and the spin transitions between the M_J states (dashed red lines) in $[DyO]^+$ calculated using the variational (panel A) and perturbative (panel B) SOC approaches.

In summary, we variationally solved the relativistic Dirac equation for the $[DyO]^+$ molecule, a prototype of Ln-based SMM. The predicted energies of the lowest M_J states were compared with those obtained with the traditional approach based on the perturbation theory applied to a solution of the Schrödinger equation corrected only for the scalar relativistic effects. The results indicate that the anisotropy barrier and the energy splittings between the M_J states depend on the interplay between strong SOC and dynamic electron correlation. This interplay affects the resonances between the spin and vibrational transitions, and, therefore, the spin relaxation time in SMMs. Without dynamic electron correlation, the variational SOC approach predicts a much larger anisotropy barrier and energy splittings between the M_J states than the traditional perturbative SOC approach. However, when the dynamic electron correlation is included, the two approaches are in better agreement. This fortunate cancelation of errors suggests that the traditional approach utilizing the perturbation theory to account for both strong SOC and dynamic electron correlation can produce reasonable results. However, this situation may not be universal for all Ln-based SMMs. Moreover, even relatively small differences in the energies of M_J states, as well as in vibrational frequencies, predicted by the variational and perturbative SOC approaches can have a large impact on the spin relaxation rate in SMMs. The presence of resonances between the spin and vibrational transitions is responsible for increasing the rate of spin relaxation.[8,50,51] Therefore, the findings of this work have important implications for predicting the spin relaxation rate in Ln-based SMMs and designing molecules with long spin relaxation time for applications in quantum information science.

THEORETICAL METHODS

The equilibrium Dy-O bond length of 1.74 Å was taken from literature.[4] The fully uncontracted dyall.cv2z basis set[52] was used in the DIRAC and GAMESS calculations, and the ANO-RCC-VDZP and ANO-RCC-VQZP basis sets[53] were used in OpenMolcas. The four-component MRCISD calculations were performed using the Dirac-Hartree-Fock molecular orbitals and the

results were compared with those calculated using the X2C method (Table S3). The two-component MRCISD calculations using the CASSCF orbitals were performed using the X2C method. All two- and four-component calculations were carried out using the DIRAC package. The computational time costs of the four- and two-component MRCISD calculations were similar, while the four-component SCF calculations were about ten times slower than the corresponding X2C calculations. Since MRCISD is much more computationally demanding than SCF, the overall time costs of four- and two-component calculations are roughly the same (see Supporting Information).The perturbative SOC calculations in GAMESS were performed using the CASCI method with the Breit-Pauli Hamiltonian[17] and the reference CASSCF wavefunction with the scalar relativistic effects described by the infinite-order two-component approach with the local unitary transformation (LUT-IOTC).[54-56] The active space was comprised of nine valence electrons of Dy^{3+} distributed over seven $4f$ orbitals. In the perturbative SOC calculations, the CASSCF wavefunction was averaged over all 2L+1=11 levels of the ^6H term of Dy^{3+}. All electronic states of $[DyO]^+$ arising from the ground levels ^6H_J (J = 15/2, 13/2 ,…, 5/2) of Dy^{3+} were included in the spin-orbit coupling Hamiltonian. The energy separation between the highest state arising from the $^6H_{15/2}$ level and the lowest state arising from the $^6H_{13/2}$ level is about 3500 cm^{-1}. Therefore, we do not expect any significant interaction between the states arising from the different levels of Dy^{3+}. In the two- and four-component variational calculations, the dynamic electron correlation was accounted for with MRCISD, while MCQDPT2 (GAMESS) and CASPT2 (OpenMolcas) methods were used in the perturbative SOC calculations. The vibrational Dy-O frequency was calculated for $M_J = \pm 15/2$ state with the X2C-CASSCF (variational SOC) and CASCI (perturbative SOC) methods. To fit the harmonic potential, the 0.005 Å step along the Dy-O distance was used to sample the energies near the equilibrium geometry.

ASSOCIATED CONTENT

Supporting Information

Computational details, molecular orbitals of $[DyO]^+$, validation of methods, details of computation time cost of variational SOC calculations, relative energies of electronic states predicted by the four- and two-component (X2C) methods, proof of vanishing spin-vibrational coupling in diatomic molecules, relative energies of electronic states predicted by the variational and perturbative SOC approaches, convergence of the X2C-MRCISD state energies with the number of virtual orbitals, comparison of the X2C-CASSCF and X2C-MRCISD state energies, comparison of the X2C-MRCISD and MCQDPT2 state energies, decomposition of electronic states in M_J components.

AUTHOR INFORMATION

ORCID

Vsevolod D. Dergachev: 0000-0001-8893-9263
Daria D. Nakritskaia: 0000-0001-8124-4223
Sergey A. Varganov: 0000-0001-8301-3891

Notes

The authors declare no competing financial interests.

ACKNOWLEDGEMENTS

This material is based upon work supported by the U.S. Department of Energy, Office of Science, Office of Basic Energy Sciences under Award Number DE-SC0022178.

REFERENCES

(1) Bogani, L.; Wernsdorfer, W. Molecular spintronics using single-molecule magnets. *Nat. Mater.* **2008**, *7*, 179–186.

(2) Rinehart, J. D.; Long, J. R. Exploiting single-ion anisotropy in the design of f-element single-molecule magnets. *Chem. Sci.* **2011**, *2*, 2078–2085.

(3) Gould, C. A.; McClain, K. R.; Reta, D.; Kragskow, J. G. C.; Marchiori, D. A.; Lachman, E.; Choi, E. S.; Analytis, J. G.; Britt, R. D.; Chilton, N. F.; Harvey, B. G.; Long, J. R. Ultrahard magnetism from mixed-valence dilanthanide complexes with metal-metal bonding. *Science* **2022**, *375*, 198–202.

(4) Ungur, L.; Chibotaru, L. F. Magnetic anisotropy in the excited states of low symmetry lanthanide complexes. *Phys. Chem. Chem. Phys.* **2011**, *13*, 20086–20090.

(5) Ungur, L.; Chibotaru, L. F. Strategies toward high-temperature lanthanide-based single-molecule magnets. *Inorg. Chem.* **2016**, *55*, 10043–10056.

(6) Ungur, L.; Chibotaru, L. F. Ab initio crystal field for lanthanides. *Chem. - A Eur. J.* **2017**, *23*, 3708–3718.

(7) Guo, F. S.; Day, B. M.; Chen, Y. C.; Tong, M. L.; Mansikkamäki, A.; Layfield, R. A. Magnetic hysteresis up to 80 Kelvin in a dysprosium metallocene single-molecule magnet. *Science* **2018**, *362*, 1400–1403.

(8) Ullah, A.; Cerdá, J.; Baldoví, J. J.; Varganov, S. A.; Aragó, J.; Gaita-Ariño, A. In silico molecular engineering of dysprosocenium-based complexes to decouple spin energy levels from molecular vibrations. *J. Phys. Chem. Lett.* **2019**, *10*, 7678–7683.

(9) Hymas, K.; Soncini, A. Molecular spintronics using single-molecule magnets under irradiation. *Phys. Rev. B* **2019**, *99*, 245404–245409.

(10) Zhu, Z.; Guo, M.; Li, X. L.; Tang, J. Molecular magnetism of lanthanide: advances and perspectives. *Coord. Chem. Rev.* **2019**, *378*, 350–364.

(11) Yin, B.; Luo, L. The anisotropy of the internal magnetic field on the centralion is capable of imposing great impact on the quantum tunneling of magnetization of Kramers single-ion magnets. *Phys. Chem. Chem. Phys.* **2021**, *23*, 3093–3105.

(12) Rocha, A. R.; García-Suárez, V. M.; Bailey, S. W.; Lambert, C. J.; Ferrer, J.; Sanvito, S. Towards molecular spintronics. *Nat. Mater.* **2005**, *4*, 335–339.

(13) Žutić, I.; Fabian, J.; Das Sarma, S. Spintronics: fundamentals and applications. *Rev. Mod. Phys.* **2004**, *76*, 323–410.

(14) Leuenberger, M. N.; Loss, D. Quantum computing in molecular magnets. *Nature* **2001**, *410*, 789–793.

(15) Mannini, M.; Pineider, F.; Sainctavit, P.; Danieli, C.; Otero, E.; Sciancalepore, C.; Talarico, A. M.; Arrio, M. A.; Cornia, A.; Gatteschi, D.; Sessoli, R. Magnetic memory of a single-molecule quantum magnet wired to a gold surface. *Nat. Mater.* **2009**, *8*, 194–197.

(16) Ermler, W. C.; Ross, R. B.; Christiansen, P. A. Spin-orbit coupling and other relativistic effects in atoms and molecules. *Adv. Quantum Chem.* **1988**, *19*, 139–182.

(17) Fedorov, D. G.; Koseki, S.; Schmidt, M. W.; Gordon, M. S. Spin-orbit coupling in molecules: chemistry beyond the adiabatic approximation. *Int. Rev. Phys. Chem.* **2003**, *22*, 551–592.

(18) Marian, C. M. Spin-orbit coupling and intersystem crossing in molecules. *Wiley Interdiscip. Rev. Comput. Mol. Sci.* **2012**, *2*, 187–203.

(19) Galitski, V.; Spielman, I. B. Spin-orbit coupling in quantum gases. *Nature* **2013**, *494*, 49–

54.
(20) Lykhin, A. O.; Kaliakin, D. S.; Depolo, G. E.; Kuzubov, A. A.; Varganov, S. A. Nonadiabatic transition state theory: application to intersystem crossings in the active sites of metal-sulfur proteins. *Int. J. Quantum Chem.* **2016**, *116*, 750–761.
(21) Marian, C. M. Understanding and controlling intersystem crossing in molecules. *Annu. Rev. Phys. Chem.* **2021**, *72*, 617–640.
(22) Dergachev, V. D.; Rooein, M.; Dergachev, I. D.; Lykhin, A. O.; Mauban, R. C.; Varganov, S. A. NAST: nonadiabatic statistical theory package for predicting kinetics of spin-dependent processes. *Top. Curr. Chem.* **2022**, *380*, 1–25.
(23) Knecht, S.; Jensen, H. J. A.; Saue, T. Relativistic quantum chemical calculations show that the uranium molecule U_2 has a quadruple bond. *Nat. Chem.* **2019**, *11*, 40–44.
(24) Lunghi, A.; Sanvito, S. How do phonons relax molecular spins? *Sci. Adv.* **2019**, *5*, 1–7.
(25) Aravena, D.; Ruiz, E. Spin dynamics in single-molecule magnets and molecular qubits. *Dalt. Trans.* **2020**, *49*, 9916–9928.
(26) Chiesa, A.; Cugini, F.; Hussain, R.; MacAluso, E.; Allodi, G.; Garlatti, E.; Giansiracusa, M.; Goodwin, C. A. P.; Ortu, F.; Reta, D.; Skelton, J. M.; Guidi, T.; Santini, P.; Solzi, M.; De Renzi, R.; Mills, D. P.; Chilton, N. F.; Carretta, S. Understanding magnetic relaxation in single-ion magnets with high blocking temperature. *Phys. Rev. B* **2020**, *101*, 174402–174409.
(27) Yin, B.; Li, C. C. A method to predict both the relaxation time of quantum tunneling of magnetization and the effective barrier of magnetic reversal for a Kramers single-ion magnet. *Phys. Chem. Chem. Phys.* **2020**, *22*, 9923–9933.
(28) Autschbach, J.; Siekierski, S.; Seth, M.; Schwerdtfeger, P.; Schwarz, W. H. E. Dependence of relativistic effects on electronic configuration in the neutral atoms of d- and f-block elements. *J. Comput. Chem.* **2002**, *23*, 804–813.
(29) Autschbach, J. Perspective: relativistic effects. *J. Chem. Phys.* **2012**, *136*, 150902–150915.
(30) Schwerdtfeger, P.; Smits, O. R.; Pyykkö, P. The Periodic Table and the physics that drives it. *Nat. Rev. Chem.* **2020**, *4*, 359–380.
(31) Saue, T.; Bast, R.; Gomes, A. S. P.; Jensen, H. J. A.; Visscher, L.; Aucar, I. A.; Di Remigio, R.; Dyall, K. G.; Eliav, E.; Fasshauer, E.; Fleig, T.; Halbert, L.; Hedegård, E. D.; Helmich-Paris, D.; Iliaš, M.; Jacob, C. R.; Knecht, S.; Laerdahl, J. K.; Vidal, M. L.; Nayak, M. K.; Olejniczak, M.; Magnus, J.; Olsen, H.; Pernpointner, M.; Senjean, B.; Shee, A.; Sunaga, A.; van Stralen, J. N. P. The DIRAC code for relativistic molecular calculations. *J. Chem. Phys.* **2020**, *152*, 204104–204117.
(32) Barysz, M.; Sadlej, A. J. Two-component methods of relativistic quantum chemistry: from the Douglas-Kroll approximation to the exact two-component formalism. *J. Mol. Struct. THEOCHEM* **2001**, *573*, 181–200.
(33) Iliaš, M.; Saue, T. An infinite-order two-component relativistic Hamiltonian by a simple one-step transformation. *J. Chem. Phys.* **2007**, *126*, 064102–064109.
(34) Liu, W.; Peng, D. Exact two-component Hamiltonians revisited. *J. Chem. Phys.* **2009**, *131*, 031104–4.
(35) Saue, T. Relativistic Hamiltonians for Chemistry: a primer. *ChemPhysChem* **2011**, *12*, 3077–3094.
(36) Cao, Z.; Li, Z.; Wang, F.; Liu, W. Combining the spin-separated exact two-component relativistic Hamiltonian with the equation-of-motion Coupled-Cluster method for the treatment of spin–orbit splittings of light and heavy elements. *Phys. Chem. Chem. Phys.*

2017, No. 3713–3721.
(37) Hu, H.; Jenkins, A. J.; Liu, H.; Kasper, Joseph, M.; Frisch, M. J.; Li, X. Relativistic two-component multireference configuration interaction method with tunable correlation space. *J. Chem. Theory Comput.* **2020**, *16*, 2975–2984.
(38) Kasper, J. M.; Li, X.; Kozimor, S. A.; Batista, E. R.; Yang, P. Relativistic effects in modeling the ligand K-edge X-ray absorption near-edge structure of uranium complexes. *J. Chem. Theory Comput.* **2022**, *18*, 2171-2179.
(39) Valentine, A. J. S.; Li, X. Intersystem crossings in late-row elements: a perspective. *J. Phys. Chem. Lett.* **2022**, *13*, 3039–3046.
(40) Schmidt, M. W.; Baldridge, K. K.; Boatz, J. A.; Elbert, S. T.; Gordon, M. S.; Jensen, J. H.; Koseki, S.; Matsunaga, N.; Nguyen, K. A.; Su, S.; Windus, T. L.; Dupius, M.; Montgomery, J . A. Jr. General Atomic and Molecular Electronic Structure System. *J. Comput. Chem.* **1993**, *14*, 1347–1363.
(41) Aquilante, F.; Autschbach, J.; Baiardi, A.; Battaglia, S.; Borin, V. A.; Chibotaru, L. F.; Conti, I.; De Vico, L.; Delcey, M.; Fdez. Galván, I.; Ferré, N.; Freitag, L.; Garavelli, M.; Gong, X.; Knecht, S.; Larsson, E. D.; Lindh, R.; Lundberg, M.; Malmqvist, P.-Å.; Nenov, A.; Norell, J.; Odelius, M.; Olivucci, M.; Pedersen, T. B.; Pedraza-González, L.; Phung, Q. M.; Pierloot, K.; Reiher, M.; Schapiro, I.; Segarra-Marti, J.; Segatta, F.; Seijo, L.; Sen, S.; Sergentu, D. C.; Stein, C. J.; Ungur, L.; Vacher, M.; Valentini, A.; Veryazov, V. Modern Quantum Chemistry with [Open]Molcas. *J. Chem. Phys.* **2020**, *152*, 214117–214125.
(42) Jensen, H. J. A.; Dyall, K. G.; Saue, T.; Faegri, K. J. Relativistic four-component multiconfigurational Self-Consistent-Field theory for molecules : formalism. *J. Chem. Phys.* **1996**, *104*, 4083–4097.
(43) Shamasundar, K. R.; Knizia, G.; Werner, H. J. A new internally contracted multi-reference configuration interaction method. *J. Chem. Phys.* **2011**, *135*, 054101–054117.
(44) Granovsky, A. A. Extended multi-configuration quasi-degenerate perturbation theory: the new approach to multi-state multi-reference perturbation theory. *J. Chem. Phys.* **2011**, *134*, 214113-14.
(45) Finley, J.; Malmqvist, P.-Å.; Roos, B. O.; Serrano-Andrés, L. The mult-state CASPT2 method. *Chem. Phys. Lett.* **1998**, *288*, 299-306.
(46) Gatteschi, D.; Sessoli, R.; Villain, J. *Molecular Nanomagnets*, 1st ed.; Oxford University Press, 2006.
(47) Etinski, M.; Tatchen, J.; Marian, C. M. Time-dependent approaches for the calculation of intersystem crossing rates. *J. Chem. Phys.* **2011**, *134*, 154105–154109.
(48) Zhang, J. M.; Liu, Y. Fermi's golden rule: its derivation and breakdown by an ideal model. *Eur. J. Phys.* **2016**, *37*, 065406–065413.
(49) Goodwin, C. A. P.; Ortu, F.; Reta, D.; Chilton, N. F.; Mills, D. P. Molecular magnetic hysteresis at 60 Kelvin in dysprosocenium. *Nature* **2017**, *548*, 439–442.
(50) Briganti, M.; Santanni, F.; Tesi, L.; Totti, F.; Sessoli, R.; Lunghi, A. A complete ab initio view of Orbach and Raman spin-lattice relaxation in a dysprosium coordination compound. *J. Am. Chem. Soc.* **2021**, *143*, 13633–13645.
(51) Reta, D.; Kragskow, J. G. C.; Chilton, N. F. Ab initio prediction of high-temperature magnetic relaxation rates in single-molecule magnets. *J. Am. Chem. Soc.* **2021**, *143*, 5943–5950.
(52) Gomes, A. S. P.; Dyall, K. G.; Visscher, L. Relativistic double-zeta, triple-zeta, and quadruple-zeta basis sets for the lanthanides La-Lu. *Theor. Chem. Acc.* **2010**, *127*, 369–381.

(53) Roos, B. O.; Lindh, R.; Malmqvist, P.-Å.; Veryazov, V.; Widmark, P.-O.; Borin, A. C. New relativistic atomic natural orbital basis sets for lanthanide atoms with applications to the Ce diatom and LuF_3 *J. Phys. Chem. A*, **2008**, *112*, 11431–11435.
(54) Barysz, M.; Sadlej, A. J. Infinite-order two-component theory for relativistic Quantum Chemistry. *J. Chem. Phys.* **2002**, *116*, 2696–2704.
(55) Seino, J.; Nakai, H. Local unitary transformation method for large-scale two-component relativistic calculations: case for a one-electron Dirac Hamiltonian. *J. Chem. Phys.* **2012**, *136*, 244102–244113.
(56) Seino, J.; Nakai, H. Local unitary transformation method for large-scale two-component relativistic calculations. II. Extension to two-electron Coulomb interaction. *J. Chem. Phys.* **2012**, *137*, 144101–144115.